JACS
JOURNAL OF THE AMERICAN CHEMICAL SOCIETY
Article
pubs.acs.org/JACS

Metal–Organic Framework Luminescence in the Yellow Gap by Codoping of the Homoleptic Imidazolate $^{3}_{\infty}$[Ba(Im)$_2$] with Divalent Europium

Jens-Christoph Rybak,[†] Michael Hailmann,[†] Philipp R. Matthes,[†] Alexander Zurawski,[†] Jörn Nitsch,[†] Andreas Steffen,[†] Joachim G. Heck,[‡] Claus Feldmann,[‡] Stefan Götzendörfer,[§] Jürgen Meinhardt,[§] Gerhard Sextl,[§] Holger Kohlmann,[∥,⊥] Stefan J. Sedlmaier,[#] Wolfgang Schnick,[#] and Klaus Müller-Buschbaum*[,†]

[†]Institut für Anorganische Chemie, Universität Würzburg, Am Hubland, 97074 Würzburg, Germany
[‡]Institut für Anorganische Chemie, Karlsruhe Institute of Technology (KIT), Engesserstr. 15, 76131 Karlsruhe, Germany
[§]Fraunhofer Institut für Silicatforschung ISC, Neunerplatz 2, 97082 Würzburg, Germany
[∥]Anorganische Festkörperchemie, Universität des Saarlandes, 66125 Saarbrücken, Germany
[⊥]Institut für Anorganische Chemie, Universität Leipzig, Johannisallee 29, 04103 Leipzig, Germany
[#]Department Chemie, Ludwig-Maximilians-Universität München, Butenandtstraße 5-13, 81377 München, Germany

Supporting Information

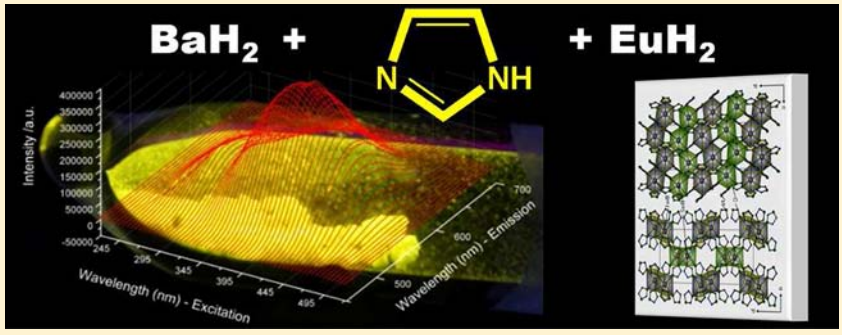

ABSTRACT: The rare case of a metal-triggered broad-band yellow emitter among inorganic–organic hybrid materials was achieved by in situ codoping of the novel imidazolate metal–organic framework $^{3}_{\infty}$[Ba(Im)$_2$] with divalent europium. The emission maximum of this dense framework is in the center of the yellow gap of primary light-emitting diode phosphors. Up to 20% Eu^{2+} can be added to replace Ba^{2+} as connectivity centers without causing observable phase segregation. High-resolution energy-dispersive X-ray spectroscopy showed that incorporation of even 30% Eu^{2+} is possible on an atomic level, with 2–10% Eu^{2+} giving the peak quantum efficiency (QE = 0.32). The yellow emission can be triggered by two processes: direct excitation of Eu^{2+} and an antenna effect of the imidazolate linkers. The emission is fully europium-centered, involving 5d → 4f transitions, and depends on the imidazolate surroundings of the metal ions. The framework can be obtained by a solvent-free in situ approach starting from barium metal, europium metal, and a melt of imidazole in a redox reaction. Better homogeneity for the distribution of the luminescence centers was achieved by utilizing the hydrides BaH_2 and EuH_2 instead of the metals.

INTRODUCTION

Metal–organic frameworks (MOFs)[1−5] exhibit remarkable properties in a growing number of fields of interest. In addition to the well-established properties of gas storage and separation,[6−12] other properties such as luminescence of MOFs has developed rapidly[13−22] to the point of the creation of white light.[21] Intrinsic luminescence renders a MOF attractive in two aspects: a combination of porosity and luminescence can be used for sensing[23−29] and also offers the opportunity of solid-state lighting (SSL) itself.[30−33] Starting from the first examples of MOFs, carboxylates are the most numerous among those frameworks and also form the largest group of luminescent MOFs, covering organic fluorescence and to some extent 4f transitions of lanthanide ions.[13−29] Besides this domination by oxo ligands, MOFs originating from chemistry utilizing amide linkers, mainly the zeolitic imidazolate frameworks (ZIFs) having structures analogous to those of zeolites that are found for metals with a coordination number of 4, have been highlighted as porous materials.[34−37] Imidazolates can also contribute to MOF luminescence in the visible range upon inclusion of lanthanide ions.[38−40] With the

Received: December 20, 2012
Published: April 12, 2013

   dx.doi.org/10.1021/ja3121718 | J. Am. Chem. Soc. 2013, 135, 6896–6902

SSL concept of doping with a low amount of luminescence centers, other metal ions such as alkaline-earth elements can be utilized as host lattice ions that are partly substituted by lanthanides.[21,39,41−44] Formation of solid solutions promotes the quantum efficiency (QE), as can be observed for green-emitting $^3_\infty[Eu_xSr_{1-x}(Im)_2]$ (x = 0.05, Im = imidazolate anion),[39] which exhibits the highest known QE for MOFs (92%) in combination with the brightness of the allowed transitions. Recent developments in SSL have focused on light-emitting diodes (LEDs), with primary LEDs based on blue or UV (Ga,In)N LEDs that excite additional phosphors of two or three colors to achieve a white-light emitter.[32,33,45,46]

It is a prominent feature of such LEDs that especially the region of wavelengths that we see as yellow light cannot be reached by (Ga,In)N systems including other elements such as Al, P, and so on. This is called the *yellow gap* of primary LEDs.[47,48] Additional phosphors such as doped oxonitridosilicates have been developed to mix blue light with green and red light in order to get good-quality white light[32,45,46] and to overcome the necessity of the elder yellow emitter YAG:Ce.[30,47,48] Because of the high variability of MOFs concerning the use of different linkers and metal ions, we can now show that MOFs can cover the complete spectrum of visible light by closing the yellow gap with the $^3_\infty[Ba(Im)_2]$:Eu^{2+} imidazolate framework, which has a spectral width comparable to that of YAG:Ce while simultaneously offering advantages such as the antenna effects of inorganic−organic hybrid materials:[49−52] the linker ligands can be used for light absorption, with subsequent energy transfer to the metal ions, which give the emission (Figure 1).

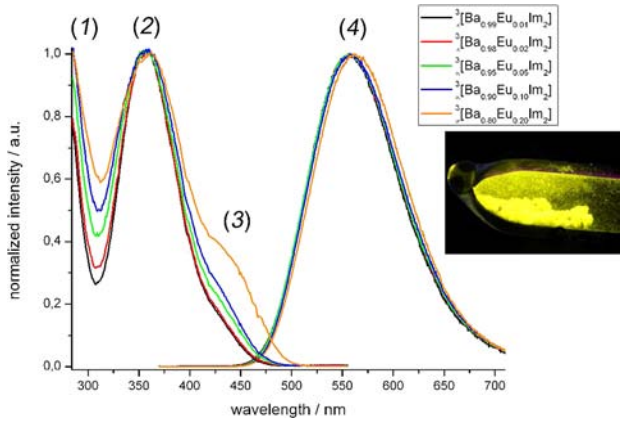

Figure 1. (left) Excitation spectra (monitored at λ_{em} = 560 nm) and (right) emission spectra (excited at λ_{exc} = 365 nm) of $^3_\infty[Ba_{1-x}Eu_x(Im)_2]$ (**1**−**5**). These yellow-emitting hybrid materials exhibit three excitation bands [labeled as (*1*)−(*3*)] as well as a broad emission band [labeled as (*4*)].

EXPERIMENTAL PROCEDURES

General Data. All manipulations were carried out under inert atmospheric conditions using glovebox, ampule, and vacuum line techniques because of air and moisture sensitivity. The microanalysis was carried out on Elementar Vario EL Cube and Vario Micro Cube analyzers. The mid-IR (MIR) spectra were recorded using a Thermo Scientific Nicolet 380 FT-IR spectrometer and KBr pellets.

Synthesis of $^3_\infty[Ba_{1-x}Eu_x(Im)_2]$ (1−5). Inidazole (37.4 mg, 0.55 mmol) was mixed with 0.25 mmol of a thoroughly ground mixture of EuH_2 and BaH_2. The mixtures were sealed in evacuated DURAN glass ampules and treated in preheated alumina tube ovens at 200 °C. The temperature was held for 18−80 h, and then the ampules were cooled to room temperature within 4 h. The reactions gave yellow powder products in yields of 86−93%. Data for **1**: Anal. Calcd for $Ba_{0.99}Eu_{0.01}C_6H_6N_4$ (M = 271.63 g mol^{-1}): C, 26.54; H, 2.23; N, 20.64%. Found: C, 27.0; H, 2.3; N, 20.4%. MIR (KBr) cm^{-1} cm^{-1}: 3432 w, 3106 vw, 3097 vw, 3082 vw, 3072 vw, 2679 vw, 2543 vw, 2442 vw, 1457 s, 1445 s, 1303 w, 1234 w, 1222 m, 1215 m, 1138 m, 1096 m, 1080 s, 1074 vs, 942 w, 924 vs, 857 w, 841 m, 826 w, 796 s, 774 s, 683 vs. Data for **2**: Anal. Calcd for $Ba_{0.98}Eu_{0.02}C_6H_6N_4$ (M = 271.77 g mol^{-1}): C, 26.53; H, 2.23; N, 20.63%. Found: C, 26.5; H, 2.2; N, 20.8%. MIR (KBr) cm^{-1}: 3105 vw, 3097 vw, 3088 w, 3083 w, 3072 vw, 2688 vw, 2542 vw, 2440 vw, 1456 s, 1445 s, 1303 m, 1245 w, 1240 w, 1234 m, 1222 s, 1214 s, 1138 s, 1104 m, 1095 m, 1080 vs, 1074 vs, 958 w, 942 m, 924 vs, 856 m, 840 s, 826 m, 796 s, 773 vs. Data for **3**: Anal. Calcd for $Ba_{0.95}Eu_{0.05}C_6H_6N_4$ (M = 272.21 g mol^{-1}): C, 26.49; H, 2.23; N, 20.60%. Found: C, 26.4; H, 2.3; N, 20.5%. MIR (KBr) cm^{-1}: 3106 vw, 3096 w, 3088 w, 3084 w, 3072 vw, 2688 vw, 2543 vw, 2441 vw, 1456 s, 1445 s, 1303 m, 1244 m, 1240 m, 1234 m, 1221 s, 1214 s, 1138 s, 1096 m, 1073 vs, 942 m, 924 vs, 856 m, 840 s, 827 m, 796 s, 772 vs. Data for **4**: Anal. Calcd for $Ba_{0.90}Eu_{0.10}C_6H_6N_4$ (M = 272.94 g mol^{-1}): C, 26.42; H, 2.22; N, 20.54%. Found: C, 26.6; H, 2.3; N, 20.4%. MIR (KBr) cm^{-1}: 3097 w, 3081 w, 3072 w, 2928 vw, 2688 vw, 2531 vw, 2442 vw, 1456 s, 1444 s, 1303 m, 1234 m, 1221 s, 1213 s, 1137 s, 1096 m, 1071 vs, 942 m, 923 vs, 855 m, 839 s, 826 m, 795 s, 769 vs. Data for **5**: Anal. Calcd for $Ba_{0.80}Eu_{0.20}C_6H_6N_4$ (M = 274.40 g mol^{-1}): C, 26.27; H, 2.21; N, 20.43%. Found: C, 26.6; H, 2.2; N, 20.0%. MIR (KBr) cm^{-1}: 3083 w, 2688 vw, 2543 vw, 2441 vw, 1456 vs, 1445 vs, 1304 m, 1245 w, 1234 w, 1222 s, 1214 s, 1137 s, 1095 s, 1072 vs, 942 m, 924 vs, 851 m, 840 s, 827 m, 796 s, 773 vs, 683 vs.

Synthesis of $^3_\infty[Ba(Im)_2]$ (6). Ba (71.4 mg, 0.52 mmol) and imidazole (74.8 mg, 1.1 mmol) were sealed in an evacuated DURAN glass ampule. The mixture was heated to 120 °C within 6 h in an alumina tube oven. The temperature was held for 72 h and then lowered to room temperature within another 2.5 h. The reaction yielded 133.5 mg (94% yield) of a colorless microcrystalline powder. Data for **6**: Anal. Calcd $BaC_6H_6N_4$ (M = 271.33 g mol^{-1}): C, 26.56; H, 2.27; N, 20.65%. Found: C, 26.9; H, 2.2; N, 20.6%. MIR (KBr) cm^{-1}: 3084 m, 2688 w, 2543 w, 2440 w, 1674 m, 1531 w, 1484 w, 1455 vs, 1446 vs, 1303 m, 1245 wsh, 1234 m, 1222 s, 1214 vs, 1138 s, 1096 ssh, 1075 vs, 942 m, 924 vs, 856 ssh, 841 s, 827 ssh, 795 s, 775 vs, 683 vs, 657 wsh.

Synthesis of BaH_2 and EuH_2. Eu ingots (99.9%) and Ba pieces (99.9%) were mechanically surface-cleaned and cut into small pieces inside an argon-filled glovebox before use. These pieces were put into crucibles machined from hydrogen-resistant Nicrofer 5219 Nb - alloy 718 and charged with hydrogen gas (99.999%, Praxair) at 280 bar in an autoclave made from the same alloy. The autoclave was heated to a temperature of 500 K for 1 day. After slow cooling to room temperature, the hydrogen pressure had decreased to 220 bar. Grinding the reaction product yielded the hydride as a white (BaH_2) or dark-red (EuH_2) fine powder.

X-ray Crystal Structure Determination of 6. $C_6H_6BaN_4$, M = 271.48 g mol^{-1}, space group $P2_1/c$, a = 9.3421(5) Å, b = 22.0982(9) Å, c = 7.6454(3) Å, β = 95.597(3)°, V = 1570.84(12) nm^3, Z = 8, ρ_{calc} = 2.2957(2) g/cm^3, STOE Stadi P diffractometer, Cu Kα_1 radiation (λ = 1.5406 Å), Debye−Scherrer geometry, T = 297 K, d range 1.80643−9.29765, 4000 data points, 276 reflections, 70 refined parameters (24 background). Investigation by powder X-ray diffraction (PXRD) showed that **1**−**5** have structures isotypic to the nondoped compound **6** (Figure S1 in the Supporting Information). The structure of **6** was solved from PXRD data exclusively. Crystallographic data are displayed in Table S1 in the Supporting Information. Structure determination was carried out using the program TOPAS-Academic 4.1.[53] Indexing of the diffraction pattern was followed by refinement of the cell and intensity extraction with the Pawley method.[54] Structure solution was done by charge flipping [55] and gave the positions of the heavy atoms as well as the approximate positions of the imidazolate anions. A structure model was created using Materials Studio software.[56] Rietveld refinement of the structure model was done with TOPAS using the fundamental parameters approach for reflection

dx.doi.org/10.1021/ja3121718 | J. Am. Chem. Soc. 2013, 135, 6896−6902

profiles (convolution of appropriate source emission profiles with axial instrument contributions as well as crystallite microstructure effects). The preferred orientation of the crystallites was described with a fourth-order spherical harmonic function. Location parameters of the Ba atoms were refined freely. The imidazolate anions were refined using rigid-body constraints, fixing the geometric arrangement of the C, N, and H atoms within each imidazolate anion but allowing free refinement of the location and orientation of the imidazolate anions themselves. Distance restraints were used to avoid unreasonably short Ba−H and H−H distances. The thermal displacement parameters of the Ba atoms were refined isotropically. Refinement of the displacement parameters of C and N atoms required constraining all atoms of one element, resulting in refinement of only one parameter for the displacement parameters of each element. Displacement parameters for H atoms were not refined. The integrity of the symmetry and geometry were checked using the program PLATON,[57] which indicated that no change of space group was necessary. See the Supporting Information for refinement details. Further information was also deposited at the Cambridge Crystallographic Data Centre (CCDC), 12 Union Road, Cambridge CB2 1EZ, U.K. (fax: +44 1223336033 or e-mail: deposit@ccdc.cam.ac.uk) and may be requested by citing the deposition number CCDC-856315, the names of the authors, and the literature citation.

SEM and EDX Analysis. The scanning electron microscopy (SEM) analysis was performed on the original powder of **5**. The powder was applied directly from an inert-gas-filled DURAN glass ampule onto an aluminum sample holder without any glue, after which the sample holder was rapidly transferred into the microscope. The powder was not sputtered with gold, platinum, or another metal to get a conductive layer (as is usual for SEM analysis) because the preparation had to be fast in order to avoid longer contact between the powder and the air. The SEM instrument used was a Zeiss ULTRA scanning electron microscope with a resolution of 1 nm at 15 kV. The pictures were made with different acceleration voltages between 2 and 20 kV with a so-called angle-selective backscattered electron (ASB) detector. This detector detects only the high-energy backscattered electrons, which are influenced not at all or to only a minor extent by any electrical charging effects. The best results were achieved at 10 kV. The white areas in the right picture in Figure 5 mark electrically charged areas. In general, it was possible to investigate the powder with only minor charging effects. The energy-dispersive X-ray spectroscopy (EDX) analysis was performed using a Sapphire Si(Li) detector from EDAX at different acceleration voltages between 5 and 30 kV.

Determination of Photoluminescence Decay, Lifetime, and Quantum Yield. All of the measurements were carried out under an inert atmosphere. Excitation and emission spectra were recorded using an Ulbricht sphere placed in a HORIBA Jobin Yvon Spex Fluorolog 3 photoluminescence spectrometer equipped with a 450 W xenon lamp, double monochromators for the excitation and emission pathways, and a R928P photomultiplier tube (PMT) as the detector. The excitation and emission spectra were fully corrected using the standard corrections supplied by the manufacturer for the spectral power of the excitation source, the reflection behavior of the Ulbricht sphere, and the sensitivity of the detector. Determination of the absolute quantum yield was performed as suggested by Friend and co-workers.[58] First, the diffuse reflection of the sample was determined under excitation (λ_{exc} = 365 nm). Second, the emission was measured for this excitation wavelength. Integration over the reflected and emitted photons using an Ulbricht sphere allows the absolute quantum yield to be calculated. In addition, the quantum yield was determined by comparison to a reference phosphor material with a known quantum yield. $BaMgAl_{10}O_{17}$:Eu (BAM), which has a quantum yield of 80% at λ_{exc} = 365 nm, was used for this purpose. The luminescence lifetimes were measured on an Edinburgh Instrument FLSP920 spectrometer via time-correlated single photon counting (TCSPC) using a 376 nm pulsed picosecond laser diode (5 mW) or a 100 W xenon microsecond flash lamp (μF920H). The emission was collected at right angles to the excitation source and detected using the R928-P PMT; the emission wavelength was selected using a double-grated monochromator. For TCSPC mode, the instrument response function (IRF) was measured using $BaSO_4$ as scattering sample with the monochromator set at the emission wavelength of the laser diode, which gave an IRF of 200 ps at 376 nm. The resulting intensity decay was a convolution of the luminescence decay with the IRF, and iterative reconvolution of the IRF with a decay function and nonlinear least-squares analysis was used to analyze the convoluted data. Measurements at 77 K were conducted in a liquid-nitrogen-cooled Oxford Instruments OptistatDN cryostat.

RESULTS AND DISCUSSION

Characterization of $^3_\infty[Ba(Im)_2]$ yielded a homoleptic dense three-dimensional (3D) framework structure, suitable as host lattice for doping with Eu^{2+} derived from a solvent-free reaction.[59,60] In addition, determination of the distribution of the luminescence centers within the host lattice and thus information on the homogeneity was obtained. As Ba^{2+} and Eu^{2+} have different cationic radii and the two frameworks are not isostructural, the formation of a complete series of solid solutions, as observed for Eu^{2+} and Sr^{2+}, is unlikely. Instead, a limited solubility of Eu in $Ba(Im)_2$ and an effect on the microscopic mixing of the cations can be observed.

In reactions starting from the metals barium and europium together with a melt of imidazole (ImH),[42] homogeneity of the products was limited by the mechanical properties of the metals, prohibiting effective mixing via grinding. Superior for the codoping of $^3_\infty[Ba(Im)_2]$ with Eu^{2+} is the reaction of BaH_2 and EuH_2 with ImH at elevated temperatures (Scheme 1). The

Scheme 1. Formation Reaction of $^3_\infty[Ba_{1-x}Eu_x(Im)_2]$ with x = 0.01 (1), 0.02 (2), 0.05 (3), 0.1 (4), 0.2 (5)

$$(1\text{-}x)\ BaH_2 + x\ EuH_2 + 2\ ImH \xrightarrow{200\ ^\circ C} {}^3_\infty[Ba_{(1-x)}Eu_x(Im)_2] + 2\ H_2$$

use of the hydrides is preferred over the use of the metals, as grinding of the hydride powders provides better homogenization of the reagents than grinding of solid metal particles.[61] In addition, formation of the known strandlike 1D coordination polymer $^1_\infty[Ba(Im)_2(ImH)_2]$ is successfully superseded, and the previously not characterized phase "$Ba(Im)_2$" becomes accessible in good crystalline quality.[42]

PXRD revealed that $^3_\infty[Ba_{1-x}Eu_x(Im)_2]$ [x = 0.01 (**1**), 0.02 (**2**), 0.05 (**3**), 0.1 (**4**), 0.2 (**5**)] crystallize isotypically in the previously unknown structure type $^3_\infty[Ba(Im)_2]$ (**6**). The structure of **6** was resolved from PXRD data after indexing and intensity extraction with the Pawley method using the charge-flipping algorithm for structure solution followed by refinement by a Rietveld fit (Figure 2).[53−55]

The crystal structure of **6** contains two different Ba^{2+} ions, each of which is surrounded by six anions, resulting in octahedral coordination polyhedra. Whereas one Ba^{2+} ion (Ba2) is σ-coordinated by six N atoms of six linking anion molecules in a μ_3-2κN^1:2κN^1:1κN^3 mode, the other Ba^{2+} ion (Ba1) is coordinated by five rings via the analogous μ_3-1κN^1:1κN^1:2κN^3 σ-N coordination mode, while the sixth ring exhibits a *T-shaped* $\sigma-\pi$ linking μ_3-1η^5:1κN^1:2κN^3 coordination mode. The structure of the framework can be described as chains of octahedra that are connected along the c axis via shared edges and bound to neighboring chains via the second N atom of the imidazolate anions to give the 3D linkage (Figure 3). The main difference relative to the Sr/Eu imidazolate framework $^3_\infty[Eu_xSr_{1-x}(Im)_2]$ is the additional η^5-π interaction.[39]

dx.doi.org/10.1021/ja3121718 | J. Am. Chem. Soc. 2013, 135, 6896−6902

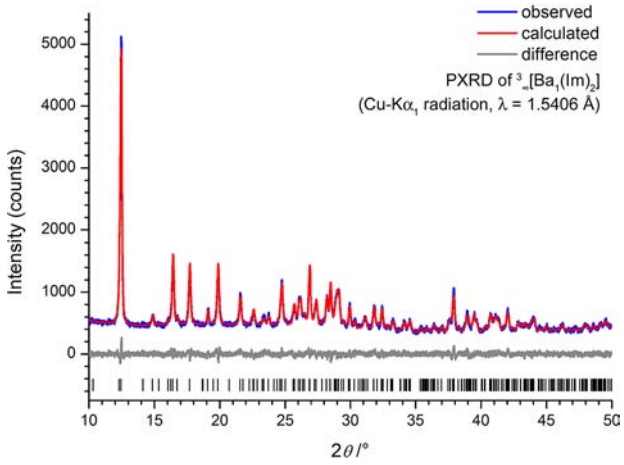

Figure 2. Rietveld refinement of PXRD data for $^3_\infty$[Ba(Im)$_2$] (**6**). The observed and calculated diffractograms are shown in blue and red, respectively. The difference plot is printed in gray, and black tick marks indicate possible reflection positions.

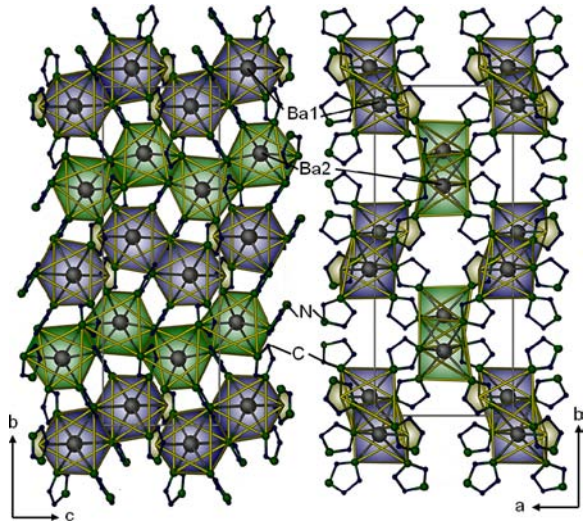

Figure 3. Crystal structure of $^3_\infty$[Ba(Im)$_2$] with views along [100] (left) and [001] (right). H atoms have been omitted for clarity. Edges of the polyhedra do not represent bonds. The η^5-π (N,C)−Ba/Eu interaction is highlighted by shading.

Although common for organometallic chemistry, such π interactions are less common for open and dense frameworks and have not been observed to date for ZIFs and other imidazolate frameworks. In accordance with the difference in the ionic radii of Ba^{2+} and Eu^{2+},[62] the increase in the coordinative demand for barium is vital and limits the amount of europium that can be doped into the host lattice to replace Ba^{2+}. Phase segregation was observed for $x > 0.2$, as monitored by PXRD and especially photoluminescence spectroscopy, which is a more sensitive detection method because of the luminescence of $^3_\infty$[Eu(Im)$_2$].[39]

Codoping with europium yields a material that exhibits strong yellow luminescence of Eu^{2+} upon excitation with UV light. Binary barium hydride doped with divalent europium, BaH_2:Eu, has recently been reported to show red luminescence due to the hydride surroundings.[61] As the emission spectra show, BaH_2:Eu was not present in the bulk product here. The bright yellow emission of $^3_\infty$[Ba$_{1-x}$Eu$_x$(Im)$_2$] derives from $4f^6 5d^1 \rightarrow 4f^7$ transitions of Eu^{2+} (Figure 1). Different from the typical parity-forbidden Ln^{3+} 4f → 4f luminescence, 5d → 4f emission is possible for divalent europium, as the crystal and ligand fields result in a reduction in the energy of the 5d states.[15,62] Thus, strong parity-allowed transitions are available in the visible range. The inclusion of 5d levels in the photoluminescence process implies broad-band transitions, as the ground and excited states differ as a function of the distance of the electrons from the core.[15,63] The emission maximum is thereby dependent on the chemical surroundings, and thus on the coordination sphere of the europium centers, and was observed at 560 nm for $^3_\infty$[Ba$_{1-x}$Eu$_x$(Im)$_2$] in **1**−**5**. The differences in the coordination of the metal cations in $^3_\infty$[Sr(Im)$_2$] and $^3_\infty$[Ba(Im)$_2$] (**6**) as well as the mismatch of the ionic radii of Eu^{2+} and Ba^{2+} are responsible for the bathochromic shift of the emission in $^3_\infty$[Ba(Im)$_2$]:Eu^{2+} (yellow, maximum 560 nm; Figure 1) relative to $^3_\infty$[Sr(Im)$_2$]:Eu^{2+} (green, maximum 510 nm; see ref 39).

Excitation of the dense framework is possible both by direct 4f → 5d Eu^{2+} excitation and by excitation of the imidazolate ligands followed by energy transfer to the metal centers. The excitation spectra show two major excitation bands and one minor excitation band. The first major excitation band [labeled (*1*) in Figure 1] has a maximum below 270 nm that can be identified as a singlet $S_0 \rightarrow S_1$ transition of the ligand.[15] The second excitation band at 365 nm [labeled as (*2*)] can be attributed to direct 4f → 5d excitation of Eu^{2+}. Additional ligand-to-metal charge transfer (LMCT) from the imidazolate ligand to Eu^{2+} as well as an $S_0 \rightarrow T_1$ transition of the imidazolate ligand can also contribute to this band,[64] as shown for terbium imidazolate.[38] Moreover, an additional long-wavelength shoulder is present at 450 nm [band (*3*)], which is presumably an europium-centered 4f → 5d transition on the second site, as it increases with an increasing europium content of the framework (orange trace in Figure 1). The luminescence lifetime was determined for $^3_\infty$[Ba$_{0.95}$Eu$_{0.05}$(Im)$_2$] (**3**) to give further insights into the participating excited states. At room temperature, the decay can be best described by a biexponential decay [τ_1 = 166(3) ns, τ_2 = 444(3) ns, λ_{exc} = 376 nm; see Table S3 in the Supporting Information), with the two components in combination with the measured quantum yield (vide infra) indicating an intrinsic lifetime of the emitting excited state of a few microseconds, as is typical for Eu^{2+}. It is feasible that the two different crystallographic environments of the europium ions give rise to the two observed lifetime components. Another possibility is that different energy transfers (i.e., different excitation pathways leading to the emitting excited state) are operative. A lifetime measurement at 77 K again gave two components [τ_1 = 357(14) ns, τ_2 = 947(4) ns, λ_{exc} = 376 nm; see Table S3], both experiencing approximately the same relative increase but a change in their contributions to the overall steady-state emission. Both factors already mentioned, namely, varying excitation pathways and europium on different crystallographic sites, can be possible explanations for this observation. A more detailed study of the energy transfer pathways and antenna effects leading to Eu^{2+} emission and multiple lifetimes in these MOFs is in progress, as we cannot rule out a combination of the multiple factors explained above.

To elaborate the efficiency of the photoluminescence process, the absolute and relative quantum yields were determined. This was especially interesting for the lower doping grades, as quenching by concentration was least expected for **1**−**3**. To address this concern, the quantum yields for all of the compounds were measured in an integrating

dx.doi.org/10.1021/ja3121718 | J. Am. Chem. Soc. 2013, 135, 6896−6902

sphere as well as by comparison to $BaMgAl_{10}O_{17}$:Eu as a reference phosphor (see the Supporting Information). The quantum yield ranged from QE = 0.28(1) to 0.32(1) at room temperature (see Table 1, which also includes chromaticity coordinates). It differed less with Eu content than in the case for $^3_\infty[Sr(Im)_2]$:Eu^{2+}, but on the other hand, the overall QE was lower than observed for the latter. The reduction in the quantum yield can be attributed to the fact that Eu^{2+} is smaller than the larger Ba^{2+} lattice site, resulting in a stronger resulting lattice distortion as well as a larger Stokes shift combined with the yellow emission. Determination of the absolute absorbance of the materials (0.57 for x = 0.01; 0.70 for x = 0.05) indicated that a higher Eu^{2+} content up to x = 0.05 resulted in an increasing brightness of the luminescence, while the QE remained unchanged. The CIE color point of the doped series **1**−**5** was almost independent of the dopant degree and centered at x = 0.433 and y = 0.516 (Figure 4 shows the position of the color point within a CIE chromaticity diagram for x = 0.1).

Table 1. Luminescence Properties of 1−3

	1	2	3
Eu^{2+} content, x	0.01	0.02	0.05
λ_{em}^{max}/nm[a]	560	560	560
CIE chromaticity point[63]			
x-coordinate	0.417	0.556	0.414
y-coordinate	0.556	0.419	0.555
absolute QE/%[a]	28(1)	32(1)	30(1)
relative QE/%[a]	25(1)	26(1)	25(1)

[a]At λ_{exc} = 365 nm.

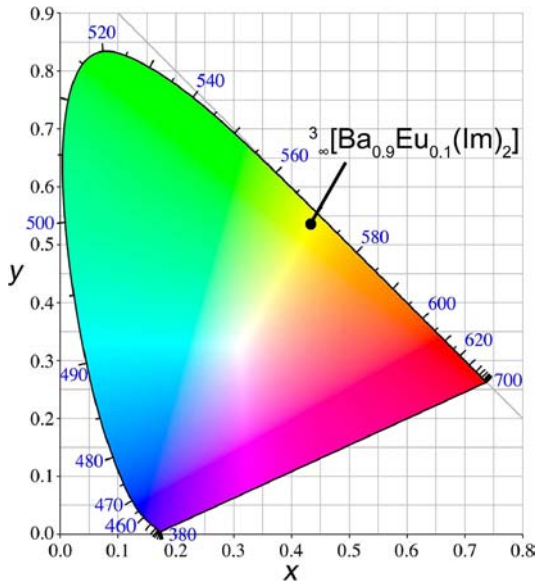

Figure 4. Chromaticity coordinate diagram of $^3_\infty[Ba_{0.9}Eu_{0.1}(Im)_2]$ (**4**) according to CIE 1931 standards.[65]

The distribution of the luminescence centers is a vital feature for a codoped material. The distribution of europium in the sample is highly influenced by the reaction conditions and sample preparation as well as the choice of precursors. For investigation of the acceptance of Eu^{2+} ions at the Ba^{2+} sites of $^3_\infty[Ba(Im)_2]$, a combination of SEM and position-dependent EDX analysis was used. Position-dependent EDX analysis was employed to study the distribution of Eu^{2+} in samples with different dopant degrees and preparation methods. Starting from a macroscopic scale (>200 μm), through multiple repetitions of overview spectra and elaboration of this to a microscopic scale (detector resolution 1 nm at 15 kV) by repeated analyses, different parts of the sample were investigated. By combination with EDX data, this was used to determine the absolute grade of dilution of dopants in the host framework. Evaluating also the microscopic distribution of the codoped luminescence centers provided additional insights, as it proved to be a significant factor to evaluate overall codoping ranges and their influence on material properties such as luminescence. For low degrees of europium doping (**1**−**3**), the distribution of the luminescence centers was unremarkable and almost ideal from hydride reactions. As macroscopic phase segregation appeared at Eu^{2+} contents higher than x = 0.2, the distribution was microscopically studied for this border value of x (i.e., compound **5**) (also see the Supporting Information). This value of x coincides in the overall result with a Ba:Eu ratio of 4:1 on a macroscopic scale. However, on a nanometer to low micrometer scale, it was found that the position-dependent distribution differed, ranging from 3.6:1 to 8.7:1. This suggests that in fact microscopically up to 28% Eu^{2+} was doped into the Ba^{2+}-containing framework at a starting constitution of 20% Eu^{2+}, with a reaction-condition-dependent gradient of the luminescence centers of 12−28% (Figure 5). In comparison, synthesis from the metals gave inhomogeneous distributions even for low dopant amounts.

It is assumed from the crystal structure of $^3_\infty[Ba(Im)_2]$ that the barium site with additional η^5 coordination is less preferable for europium incorporation, whereas the non-π-coordinated site is preferred as it resembles the coordination in $^3_\infty[Eu(Im)_2]$.[39] Reasons for phase segregation at higher Eu^{2+} contents (but lower than the fraction of the preferable Ba site, 0.5) can be found in the coordinative differences of the parent structures, the mismatch in ionic radii, and finally the scale of the macroscopic particles of the hydrides that were used as reagents (400 nm to 250 μm). Their initial extensions can easily lead to small single-ion-dominated islands at the start of the MOF formation. The concentration gradient between the barium-majority parts and the europium-majority parts is reduced throughout the reaction via migration of the cations. The combination of SEM with position-dependent EDX analysis showed that no equilibrium was reached concerning the cation migration for $x \geq 0.2$ (see Figure 5 and the Supporting Information). This coincides with the appearance of two types of crystal sizes that are found in the product: larger crystals (10 to 400 μm) that have a higher barium and lower europium content (7.8:1 to 8.7:1) than the overall macroscopic constitution and smaller crystals (50 nm to 10 μm that exhibit a higher europium and a lower barium content (3.6:1 to 4.1:1). As neither show a diffraction pattern nor emission of $^3_\infty[Eu(Im)_2]$, we conclude that both still have to be described by the formula $^3_\infty[Ba_{1-x}Eu_x(Im)_2]$ but as a nonideal solid solution.

It can be concluded that the distribution of the luminescence centers also affects the efficiency of the luminescence of the MOF material. Low acceptance and clustering of the luminescence centers favor cross-relaxation processes. This leads to quenching by concentration apart from the overall dopant amount. This also corroborates the observation that the quantum yields are stable and almost identical for the well-

dx.doi.org/10.1021/ja3121718 | J. Am. Chem. Soc. 2013, 135, 6896−6902

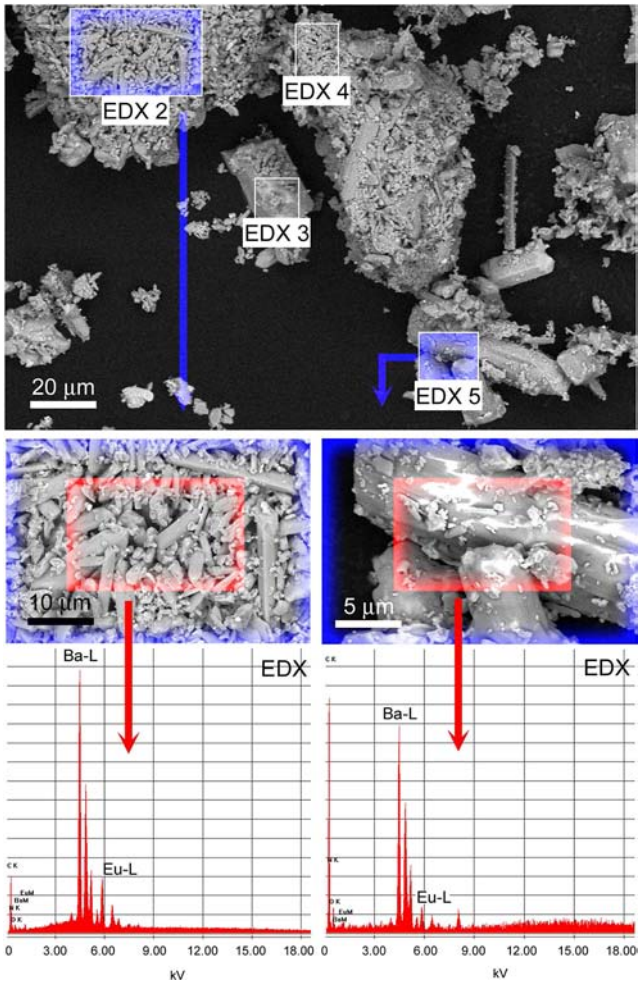

Figure 5. (top) SEM and (bottom) position-dependent EDX analysis of ${}^{3}_{\infty}[Ba_{0.8}Eu_{0.2}(Im)_2]$ (**5**) illustrating the presence of Eu-rich (28%) (EDX 2 and 4) and Ba-rich (87%) (EDX 3 and 5) microscopic parts of the product that coincide with microcrystals of different size and shape (detector resolution 1 nm at 15 kV).

distributed low amounts of Eu^{2+} dopant in **1**−**3** (x = 0.01−0.05).

CONCLUSIONS

We have reported a novel dense framework material, ${}^{3}_{\infty}[Ba(Im)_2]:Eu^{2+}$, featuring intrinsic luminescence in the yellow gap of primary LED phosphors, that was formed by codoping of the barium-containing imidazolate host lattice with divalent europium. To the best of our knowledge, this is the first MOF with luminescence in the center of the yellow gap of primary LEDs. It is hereby proven that MOFs can cover the complete visible range of colors by photoluminescence, as blue, green, and red were known already. As a general insight, codoping of the imidazolate host lattice with different cations as luminescence centers under exchange of the connectivity points enables bright, tunable emission. Upon doping with divalent europium, the emission derives from 5d → 4f transitions and is dependent on the chemical surroundings, which is a major difference in comparison with the 4f → 4f transitions of trivalent lanthanide ions. Mismatches in the ionic radii of the cations together with other factors such as the synthesis conditions limit the acceptance of the host lattice and the distribution of the luminescence centers. The use of the hydrides BaH_2 and EuH_2 enables in situ doping during synthesis of the framework that allows higher degrees of doping on a microscopic level than indicated by the macroscopic ratio of the reagents and positively influences the distribution of the luminescence centers. As the grade of distribution is supposed to have a beneficial effect on the efficiency of the luminescence, clustering of the luminescence centers is thereby kept low. Because of similar quantum yields for Eu^{2+} content (x) between 0.01 and 0.05, the absolute absorbance and thereby the brightness of the materials increase with increasing x. Microscopic determination of the distribution of luminescence centers has provided important insights into the codoping of MOFs as hybrid materials.

ASSOCIATED CONTENT

Supporting Information

Experimental details, crystallographic data (CIF), and PXRD and photoluminescence data. This material is available free of charge via the Internet at http://pubs.acs.org.

AUTHOR INFORMATION

Corresponding Author

k.mueller-buschbaum@uni-wuerzburg.de

Notes

The authors declare no competing financial interest.

ACKNOWLEDGMENTS

This work was supported by the Deutsche Forschungsgemeinschaft and the Dr. Klaus Römer Foundation.

REFERENCES

(1) Hoskins, B. F.; Robson, R. *J. Am. Chem. Soc.* **1989**, *111*, 5962−5964.
(2) Kitagawa, S.; Kondo, M. *Bull. Chem. Soc. Jpn.* **1998**, *71*, 1739−1753.
(3) Li, H.; Eddaoudi, M.; O'Keeffe, M.; Yaghi, O. M. *Nature* **1999**, *402*, 276−279.
(4) Serre, C.; Millange, F.; Thouvenot, C.; Noguès, M.; Marsolier, G.; Louër, D.; Férey, G. *J. Am. Chem. Soc.* **2002**, *124*, 13519−13526.
(5) Eddaoudi, M.; Moler, D. B.; Li, H.; Chen, B.; Reineke, T. M.; O'Keeffe, M.; Yaghi, O. M. *Acc. Chem. Res.* **2001**, *34*, 319−330.
(6) Rowsell, J. L. C.; Yaghi, O. M. *Microporous Mesoporous Mater.* **2004**, *73*, 3−14.
(7) Tan, C.; Yang, S.; Champness, N. R.; Lin, X.; Blake, A. J.; Lewis, W.; Schröder, M. *Chem. Commun.* **2011**, *47*, 4487−4489.
(8) Murray, L. J.; Dincă, M.; Long, J. R. *Chem. Soc. Rev.* **2009**, *38*, 1294−1314.
(9) Matsuda, R.; Kitaura, R.; Kitagawa, S.; Kubota, Y.; Belosludov, R. V.; Kobayashi, T. C.; Sakamoto, H.; Chiba, T.; Takata, M.; Kawazoe, Y.; Mita, Y. *Nature* **2005**, *436*, 238−241.
(10) Mueller, U.; Schubert, M.; Teich, F.; Puetter, H.; Schierle-Arndt, K.; Pastré, J. *J. Mater. Chem.* **2006**, *16*, 626−636.
(11) Li, J.-R.; Ma, Y.; McCarthy, M. C.; Sculley, J.; Yu, J.; Jeong, H.-K.; Balbuena, P. B.; Zhou, H.-C. *Coord. Chem. Rev.* **2011**, *255*, 1791−1823.
(12) Li, J.-R.; Kuppler, R. J.; Zhou, H.-C. *Chem. Soc. Rev.* **2009**, *38*, 1477−1504.
(13) Allendorf, M. D.; Bauer, C. A.; Bhakta, R. K.; Houk, R. J. T. *Chem. Soc. Rev.* **2009**, *39*, 1330−1352.
(14) Rocha, J.; Carlos, L. D.; Almeida Paz, F. A.; Ananias, D. *Chem. Soc. Rev.* **2011**, *40*, 926−940.
(15) Binnemans, K. *Chem. Rev.* **2009**, *109*, 4283−4374.
(16) Janiak, C.; Vieth, J. K. *New J. Chem.* **2010**, *34*, 2366−2388.
(17) Serre, C.; Millange, F.; Thouvenot, C.; Gardant, N.; Pelle, F.; Férey, G. *J. Mater. Chem.* **2004**, *14*, 1540−1543.

(18) Ye, J.-W.; Wang, J.; Zhang, J.-Y.; Zhang, P.; Wang, Y. *CrystEngComm* **2007**, *9*, 515−523.
(19) Höller, C. J.; Mai, M.; Feldmann, C.; Müller-Buschbaum, K. *Dalton Trans.* **2010**, *39*, 461−468.
(20) Guo, J.; Ma, J.-F.; Liu, B.; Kan, W.-Q.; Yang, J. *Cryst. Growth Des.* **2011**, *11*, 3609−3621.
(21) Sava, D. F.; Rohwer, L. E. S.; Rodriguez, M. A.; Nenoff, T. M. *J. Am. Chem. Soc.* **2012**, *134*, 3983−3986.
(22) Matthes, P. R.; Höller, C. J.; Mai, M.; Heck, J.; Schmiechen, S.; Sedlmaier, S.; Feldmann, C.; Schnick, W.; Müller-Buschbaum, K. *J. Mater. Chem.* **2012**, *22*, 10179−10187.
(23) Bauer, C. A.; Timofeeva, T. V.; Settersten, T. B.; Patterson, B. D.; Liu, V. H.; Simmons, B. A.; Allendorf, M. D. *J. Am. Chem. Soc.* **2007**, *129*, 7136−7144.
(24) Chen, B.; Yang, Y.; Zapata, F.; Lin, G.; Qian, G.; Lobkovsky, E. B. *Adv. Mater.* **2007**, *19*, 1693−1696.
(25) Harbuzaru, B. V.; Corma, A.; Rey, F.; Atienzar, P.; Jorda, J. L.; Garcia, H.; Carlos, L. D.; Rocha, J. *Angew. Chem., Int. Ed.* **2008**, *47*, 1080−1083.
(26) Lan, A.; Li, K.; Wu, H.; Olson, D. H.; Emge, T. J.; Ki, W.; Hong, M.; Li, J. *Angew. Chem., Int. Ed.* **2009**, *48*, 2334−2338.
(27) Cui, Y.; Xu, H.; Yue, Y.; Guo, Z.; Yu, J.; Chen, Z.; Gao, J.; Yang, Y.; Qian, G.; Chen, B. *J. Am. Chem. Soc.* **2012**, *134*, 3979−3982.
(28) Feng, P. L.; Leong, K.; Allendorf, M. D. *Dalton Trans.* **2012**, *41*, 8869−8877.
(29) Chen, L.; Tan, K.; Lan, Y.-Q.; Li, S.-L.; Shao, K.-Z.; Su, Z.-M. *Chem. Commun.* **2012**, *48*, 5919−5921.
(30) Nakamura, S. *Proc. Soc. Photo-Opt. Instrum. Eng.* **1997**, *3002*, 26−35.
(31) Mueller-Mach, R.; Mueller, G. O.; Krames, M. R.; Trottier, T. *IEEE J. Sel. Top. Quantum Electron.* **2002**, *8*, 339−345.
(32) Mueller-Mach, R.; Mueller, G. O.; Krames, M. R.; Hoppe, H. A.; Stadler, F.; Schnick, W.; Juestel, T.; Schmidt, P. *Phys. Status Solidi A* **2005**, *202*, 1727−1732.
(33) Phillips, J. M.; Coltrin, M. E.; Crawford, M. H.; Fischer, A. J.; Krames, M. R.; Mueller-Mach, R.; Mueller, G. O.; Ohno, Y.; Rohwer, L. E. S.; Simmons, J. A.; Tsao, J. Y. *Laser Photonics Rev.* **2007**, *1*, 307−333.
(34) Park, K. S.; Ni, Z.; Côté, A. P.; Choi, J. Y.; Huang, R. D.; Uribe-Romo, F. J.; Chae, H. K.; O'Keeffe, M.; Yaghi, O. M. *Proc. Natl. Acad. Sci. U.S.A.* **2006**, *103*, 10186−10191.
(35) Wang, B.; Côté, A. P.; Furukawa, H.; O'Keeffe, M.; Yaghi, O. M. *Nature* **2008**, *453*, 207−211.
(36) Banerjee, R.; Phan, A.; Wang, B.; Knobler, C. B.; Furukawa, H.; O'Keeffe, M.; Yaghi, O. M. *Science* **2008**, *319*, 939−943.
(37) Phan, A.; Doonan, C. J.; Uribe-Romo, F. J.; Knobler, C. B.; O'Keeffe, M.; Yaghi, O. M. *Acc. Chem. Res.* **2010**, *43*, 58−67.
(38) Müller-Buschbaum, K.; Torres, S. G.; Larsen, P.; Wickleder, C. *Chem. Mater.* **2007**, *19*, 655−659.
(39) Zurawski, A.; Mai, M.; Baumann, D.; Feldmann, C.; Müller-Buschbaum, K. *Chem. Commun.* **2011**, *47*, 496−498.
(40) Müller-Buschbaum, K. *Z. Naturforsch.* **2006**, *61b*, 792−797.
(41) Falcaro, P.; Furukawa, S. *Angew. Chem., Int. Ed.* **2012**, *51*, 8431−8433.
(42) Zurawski, A.; Rybak, J.-C.; Meyer, L. V.; Matthes, P. R.; Stepanenko, V.; Dannenbauer, N.; Würthner, F.; Müller-Buschbaum, K. *Dalton Trans.* **2012**, *41*, 4067−4078.
(43) Ablet, A.; Li, S.-M.; Cao, W.; Zheng, X.-J.; Wong, W.-T.; Jin, L.-P. *Chem.—Asian J.* **2013**, *8*, 95−100.
(44) Zhang, W.; Yu, J.; Cui, Y.; Rao, X.; Yang, Y.; Qian, G. *J. Alloys Compd.* **2013**, *551*, 616−620.
(45) Bachmann, V.; Ronda, C.; Oeckler, O.; Schnick, W.; Meijerink, A. *Chem. Mater.* **2009**, *21*, 316−325.
(46) Nägele, T. *LED Prof. Rev.* **2008**, *10*, 1−3.
(47) Nakamura, S.; Mukai, T.; Senoh, M. *Jpn. J. Appl. Phys.* **1992**, *31*, 1258−1266.
(48) Schubert, E. F. *Light-Emitting Diodes*; Cambridge University Press: Cambridge, U.K., 2006.
(49) Weissman, S. I. *J. Chem. Phys.* **1942**, *10*, 214−217.
(50) Batista, H. J.; de Andrade, A. V. M.; Longo, R. L.; Simas, A. M.; de Sá, G. F.; Ito, N. K.; Thompson, L. C. *Inorg. Chem.* **1998**, *37*, 3542−3547.
(51) Sabbatini, N.; Guardigli, M.; Lehn, J.-M. *Coord. Chem. Rev.* **1993**, *123*, 201−228.
(52) Zhang, X.; Ballem, M. A.; Hu, Z.-J.; Bergman, P.; Uvdal, K. *Angew. Chem., Int. Ed.* **2011**, *50*, 5729−5733.
(53) Coelho, A. *TOPAS-Academic*, version 4.1; Coelho Software: Brisbane, Australia, 2007.
(54) Pawley, G. S. *J. Appl. Crystallogr.* **1981**, *14*, 357−361.
(55) Oszlányi, G.; Sütő, A. *Acta Crystallogr.* **2004**, *A60*, 134−141.
(56) *Materials Studio*, version 5.5.0.0; Accelrys Software Inc.: San Diego, CA, 2010.
(57) Spek, A. L. *PLATON-2000: A Multipurpose Crystallographic Tool*, version 1.07; University of Utrecht: Utrecht, The Netherlands, 2003.
(58) de Mello, J. V.; Wittmann, H. F.; Friend, R. H. *Adv. Mater.* **1997**, *9*, 230−232.
(59) Müller-Buschbaum, K.; Mokaddem, Y.; Schappacher, F.; Pöttgen, R. *Angew. Chem., Int. Ed.* **2007**, *46*, 4385−4387.
(60) See the Supporting Information for further characterization.
(61) Kunkel, N.; Kohlmann, H.; Sayede, A.; Springborg, M. *Inorg. Chem.* **2011**, *50*, 5873−5875.
(62) Shannon, R. D. *Acta Crystallogr.* **1976**, *A32*, 751−767.
(63) Blasse, G.; Grabmeier, B. C. *Luminescent Materials*; Springer: Berlin, 1994; pp 41−50.
(64) Machado, F. B. C.; Davidson, E. R. *J. Chem. Phys.* **1992**, *97*, 1881−1891.
(65) *Phosphor Handbook*; Shionoya, S., Yen, W. M., Eds.; CRC Press: Boca Raton, FL, 1999.